N91-26618

Chapter 5

Data Acquisition and processing

Toshitaka Tsuda

Radio Atmospheric Science Center, Kyoto University

1 INTRODUCTION

This chapter is devoted to describing fundamental methods of signal processing used in normal MST radar observations. Complex time series of received signals obtained in each range gate are converted into Doppler spectra, from which the mean Doppler shift, spectral width and signal-to-noise ratio (SNR) are estimated. These spectral parameters are further utilized to study characteristics of scatterers and atmospheric motions.

Since it is beyond a scope of this note to describe general techniques developed in radar engineering, readers are encouraged to study a comprehensive textbooks on modern radar techniques such as *Cook and Bernfeld* [1967], *Barton* [1976], *Skolnik* [1981]. Fundamental and advanced techniques of digital signal processing are also summarized by *Gold and Rader* [1969] and *Bendat and Piersol* [1971].

Detailed descriptions of clear air radars operating at frequencies ranging from VHF to a microwave are given by *Gossard and Strauch* [1983] and *Doviak and Zrnić* [1984]. General MST radar techniques are also reviewed by many authors [e.g., *Gage and Balsley*, 1978].

2 RECEIVER HARDWARE

Fig. 1 schematically shows the simplified structure of an MST radar system and the flow of received signals. A VHF or UHF sine wave carrier generated by a stable oscillator is modulated by a rectangular pulse with a width of a few microseconds. This is commonly called a pulsed continuous wave (CW). The transmitted radio wave is backscattered toward the radar. The radar echo is fed to a receiver system through a TR-switch that protects the receiver from damage caused by the high power of the transmitter during the transmission. The received RF signal, which is usually a replica of the transmitted signal, is pre-amplified by a radio frequency (RF) amplifier. The RF signal is mixed with a coherent local (LO) signal and is down-converted to an intermediate frequency (IF) signal.

After maximizing the peak-signal-to-noise power ratio in the IF amplifier, the IF signal is detected by a quadrature detector, which produces a time series of sine and cosine components of the received signal. The detected signal is finally converted to digital signal by an analogue-to-digital (AD) converter, then transferred to a digital signal processing system.

The pulse may be compressed by phase modulation, which is decoded before or after the AD conversion by an analogue or digital correlator, respectively.

3 MATCHED FILTER

The IF-amplifier is generally regarded as a filter with gain, which should be designed to maximize the peak signal-to-noise power ratio SNR_P. Note that the peak signal power defined here corresponds to the maximum instantaneous power, and not to the integrated signal power within the bandwidth. Thus, the SNR_P is not equal to the SNR, which is a

ratio of the integrated signal power to the integrated noise power within the bandwidth. The latter is used in later sections.
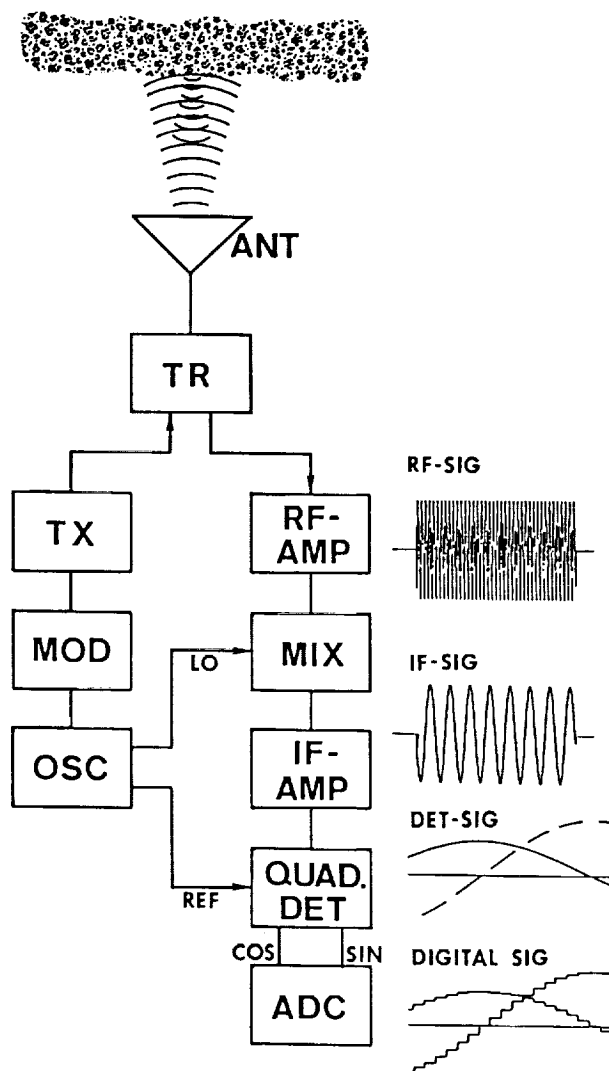

Fig. 1. Block diagram of a typical MST radar system, together with signal waveforms.

Fig.2 shows typical frequency spectra of a pulsed CW signal with a width (duration) τ and of noise. The former is approximated by

$$(\frac{\sin(2\pi \hat{f}/2)}{2\pi \hat{f}/2})^2 \tag{1}$$

where $\hat{f}$ is a frequency normalized by $1/\tau$, while the noise can be considered to be white, i.e., its intensity is statically independent of frequency. Although the received signal contains many Fourier spectral components, the receiver amplifies only components that are within a finite bandwidth.
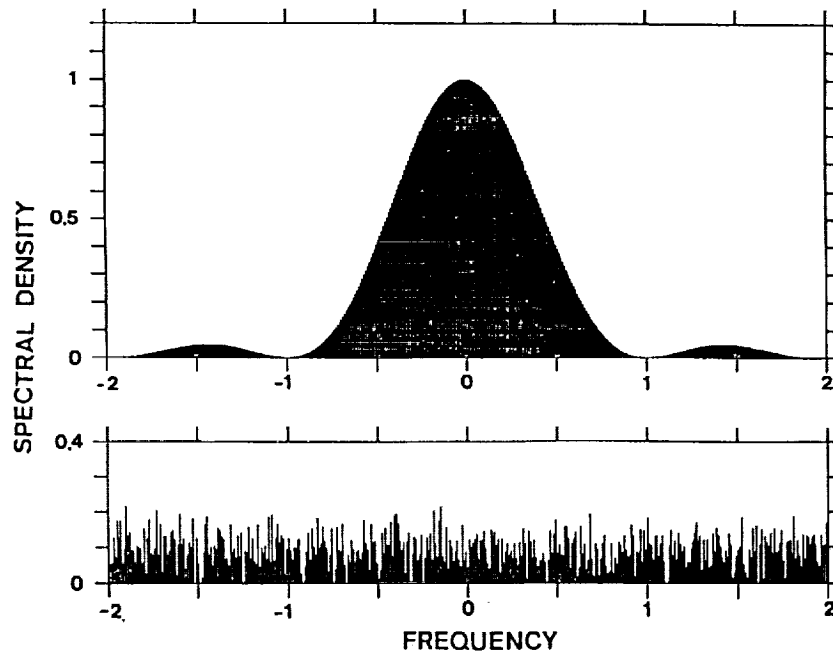

Fig. 2. Frequency spectrum of a pulsed CW signal (top panel) and white noise (bottom panel). The frequency is normalized by the inverse of the rectangular pulse width.

Fig. 3 shows the integrated power of the signal and noise spectra shown in Fig. 2 as a function of double-sided bandwidth B. Since noise spectral density is distributed uniformly in the frequency range of the signal, the integrated noise power is proportional to the receiver bandwidth B. On the other hand, the signal power increases rapidly when B is small, then approaches a constant value as B becomes larger.

When B is considerably narrower than the bandwidth occupied by the signal, the signal energy is not effectively detected by the signal processing, although the noise energy is reduced. On the other hand, if B is wide compared with the signal bandwidth, extraneous noise is introduced by the excess bandwidth, which lowers the output SNR_P. Thus, there is an optimum bandwidth depending on the signal spectrum.
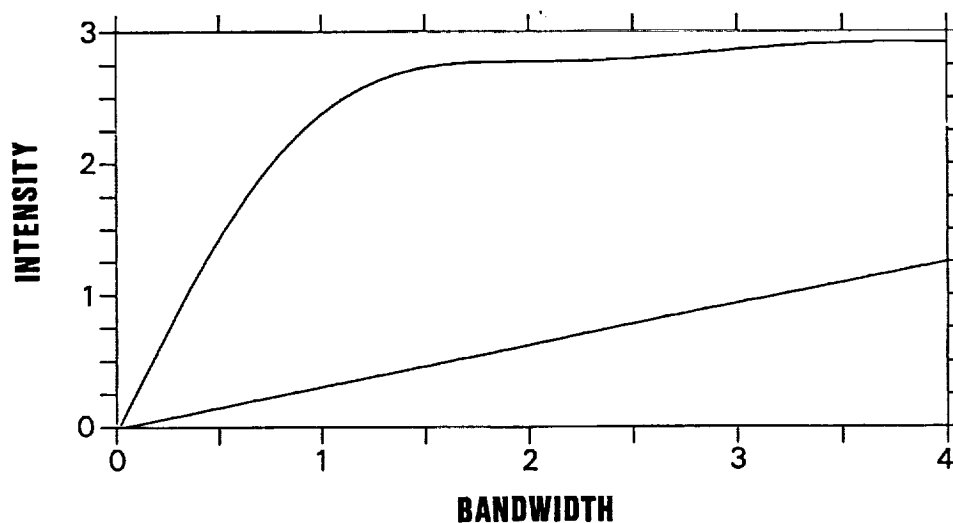

Fig. 3. Integrated power of the signal (upper curve) and noise (lower curve) spectra shown in Fig. 2. The bandwidth is a double-sided frequency range.

The optimum filter is obtained by applying a matched filter design [e.g., *Barton*, 1976; *Skolnik*, 1981], which is generally defined as a network whose frequency-response function is matched to the pre-filter signal spectrum in order to maximize SNR_P.

The frequency-response function of the IF-amplifier $H(f)$ specifies the relative amplitude and phase of the output signal with respect to the input when the input is a pure sinusoid. For a received signal voltage spectrum $S(f)$, $H(f)$ for the matched filter can be expressed as

$$H(f) = G_a S^*(f) \exp(-i2\pi f t_d) \tag{2}$$

where G_a and t_d are the gain of the network and the time delay. $H(f)$ is the complex conjugate of the signal spectrum except for a phase shift due to the time delay.

As a result, the normalized amplitude spectrum of the matched filter, which corresponds to the filter passband characteristics, is the same as the amplitude spectrum of the signal, but the phase spectrum of the matched filter is the negative of the phase spectrum of the signal plus a phase shift proportional to frequency. By using phase spectra $\phi_S(f)$ and $\phi_H(f)$ for the signal and matched filter, respectively, Eq. (2) can be rewritten as follows:

$$|H(f)| = |S(f)|$$

$$\phi_H(f) = -\phi_S(f) + 2\pi f t_d \tag{3}$$

Specification of the optimum receiver characteristics involves the frequency-response function and the shape of the received waveform, which is usually a replica of the transmitted signal spectrum. The transmitted signal spectrum is usually tapered from the spectrum of a rectangular pulsed CW in order to suppress harmonics and spurious transmission. Therefore, the matched filter design largely depends on the transmitter characteristics.

It is often impractical to construct the exact matched filter. If the signal wave form

is a rectangular pulsed CW, to simplify the filter hardware the matched filter for the IF-amplifier is approximated by a band-pass filter (BPF). The optimum IF bandwidth B_{IF} is the order of $1/\tau$. More precisely, it can be shown that B_{IF} should be $1.4/\tau$ for the optimum rectangular filter.

4   OUTLINE OF A DIGITAL PROCESSING SYSTEM

Fig. 4 shows the flow of the signal processing for a digital signal transferred from the receiver. This processing can be done either in real-time or in an off-line computation, depending on the capability of the system-installed computer system.

```
                    ┌─────────────┐
                    │  RECEIVED   │
                    │   SIGNAL    │
                    └─────────────┘
                           │
                    ┌─────────────┐
                    │   RANGING   │
                    │ (SAMPLING)  │
                    └─────────────┘
                           │
              ┌──────────────────────┐
              │  COHERENT INTEGRATION │
              │ (TIME-DOMAIN AVERAGING)│
              └──────────────────────┘
                           │
               ┌─────────────────────┐
               │  SPECTRAL ANALYSIS  │
               │ (FOURIER TRANSFORM) │
               └─────────────────────┘
                           │
              ┌──────────────────────┐
              │ INCOHERENT INTEGRATION│
              │ (SPECTRAL AVERAGING)  │
              └──────────────────────┘
                           │
                    ┌─────────────┐
                    │ NOISE LEVEL │
                    │ ESTIMATION  │
                    └─────────────┘
                           │
               ┌─────────────────────┐
               │ SPECTRAL PARAMETER  │
               │    ESTIMATION       │
               └─────────────────────┘
                           │
                    ┌─────────────┐
                    │ ECHO POWER  │
                    │DOPPLER SHIFT│
                    │SPECTRAL WIDTH│
                    └─────────────┘
```
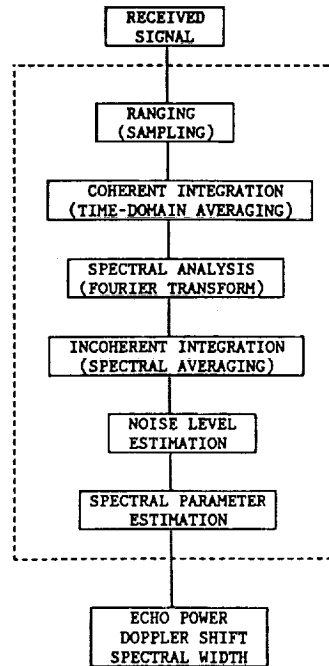
Fig. 4. Flow diagram of a typical digital signal processing system.

The sampled digital signal is arranged as a function of a round-trip time from transmission to reception, which is generally called ranging, and is coherently integrated in order to increase a signal-to-noise ratio SNR. The complex time series of the received signal is Fourier transformed into Doppler spectra. After incoherently averaging the Doppler spectra, the noise level is estimated. Spectral parameters such as the SNR, mean Doppler shift and spectral width are estimated from the Doppler spectra. They are usually stored in a mass storage system for further analysis of radar reflectivity, wind fields and turbulence parameters.

5 RANGING

For a monostatic pulse radar, the distance, or range R to the scatterer from the radar becomes

$$R = \frac{cT_R}{2} \tag{4}$$

where c is the speed of light $c = 3 \times 10^8$ m/s, and T_R is the time interval between the pulse transmission and detection. The denominator 2 appears in (4) because T_R corresponds to the round-trip time interval for radio wave propagation over the range R. In convenient units (4) becomes

$$R(\text{km}) = 0.15 T_R(\mu s) \tag{5}$$

Fig. 5 schematically shows a time-height chart between the range and the round-trip time interval for a radar echo. The interval t_{IPP} between successive pulse transmissions is called the inter-pulse-period (IPP), and the corresponding frequency is called the pulse repetition frequency (PRF). Normally MST radars are operated with uniform IPP, which is, for an example, set equal to 1 ms in Fig. 5. H_m in Fig. 5 is defined as $ct_{IPP}/2$.

The SNR is linearly dependent on the average transmitted power in the IPP. Therefore, in order to increase the SNR, the IPP should be as short as possible when the pulse length and peak transmitting power are fixed. On the other hand, a sufficient length of time must elapse after a pulse is transmitted in order to receive all of the radar echoes before the transmission of the next pulse. Thus, the IPP is determined primarily by the longest range at which targets are expected.
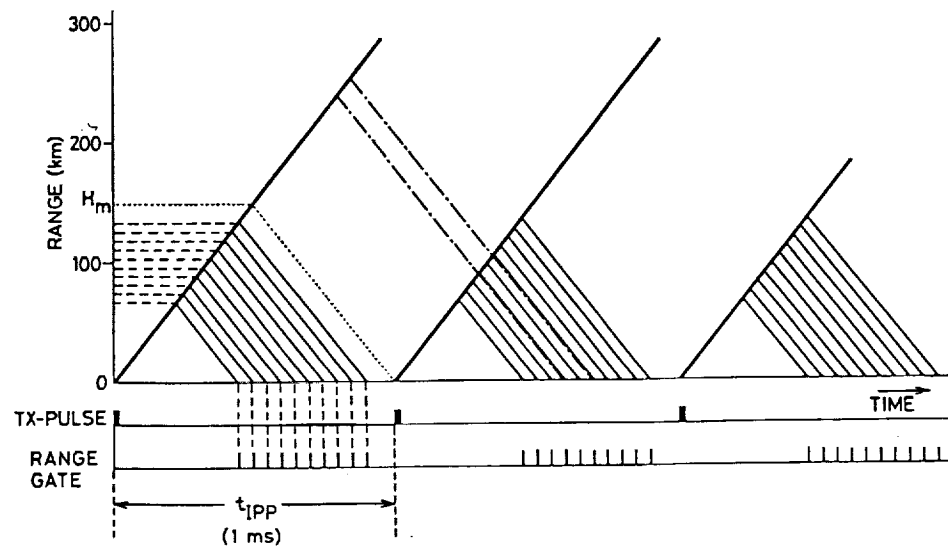

Fig. 5. Time-height chart for MST radar observations when when IPP is 1 ms. Thick and thin solid lines correspond to propagation of transmitted and scattered radiowaves, respectively. The received signal is sampled 10 times with equally spaced range gates as indicated by the dash lines. The dot-dash lines show a second-time-around echoes due to ionospheric scattering.

If the IPP is too short, echo signals from some targets might arrive after the transmission of the next pulse, as indicated by the dot-dash lines in Fig. 5. These echoes from a range greater than $ct_{IPP}/2$ are received during the same interval that as echoes from targets nearer than $ct_{IPP}/2$ return echoes from the next pulse. As a result, instead of their actual range R, they appear to have a range $R - H_m$ or R minus a multiple of H_m.

This ambiguity in the ranging is called a range aliasing. Signals that arrive after the transmission of the next pulse are generally called second-time-around (or multiple-time-around) echoes. The range H_m is called the maximum unambiguous range, beyond which targets appear as second-time-around echoes.

Fig. 6. Time-height chart for an MST radar whose antenna beam is steered every IPP into three directions as shown in the right panel.

For normal MST radar observations, clear air echoes are usually detected at heights lower than 100 km, which corresponds to $t_{IPP} = 667\mu s$. So, the IPP is usually set equal to less than 1 ms. Then, echoes scattered from the ionosphere would be received as shown in Fig. 5. These can be considered as a kind of multiple-time-around echoes, although characteristics of radar echoes are fairly different between the first and multiple-time-around echoes. The normal ionospheric echoes are much weaker than the clear air echoes and have much a broader spectral distribution, therefore, they may instead act as a white noise added to the normal cosmic noise. Although range-aliased ionospheric echoes increase the noise level, depending on the electron density, they do not usually present a large problem in estimating the spectral parameters of the Doppler spectra when the SNR is significantly large.

However, the intense radar echoes that are sometimes received from ionospheric irregularities such as sporadic E layers or meteor trails may seriously contaminate the clear air echoes. In such cases, t_{IPP} should be made large enough to remove the range aliasing.

Another way to weaken the effects of range aliasing is to change the antenna beam direction between every pulse. Fig. 6 shows the time-height chart for an MST radar that is steered sequentially into three directions, eastward, vertical and southward, denoted 1, 2 and 3. Thus, the effective IPP in each beam direction becomes three times the original IPP, which is usually large enough to remove the multiple-time-around echoes from the ionosphere. Of course, this technique can only be used with a directionally agile radar such as the MU radar [Kato et al., 1984].

6 RADAR SAMPLING VOLUME

Normal MST radar observations assume that the volume illuminated by the radar antenna beam is filled with scatterers. Fig. 7 schematically shows transmission and reception of a purely rectangular pulse with a width τ. The leading edge of the transmitted pulse covers distances from z_0 to $z_0 + c\tau/2$, while the tail end of the pulse goes from $z_0 - c\tau/2$ to z_0. In total, the sampling volume extends from $z_0 - c\tau/2$ to $z_0 + c\tau/2$ with a thickness of $c\tau$. The right panel in Fig. 7 shows that the weighting function of the sampling volume has a triangular distribution partly overlapping the weighting function of the adjacent upper and lower sampling volumes. The range resolution is usually expressed as $c\tau/2$, which corresponds to the half power width of the weighting function.
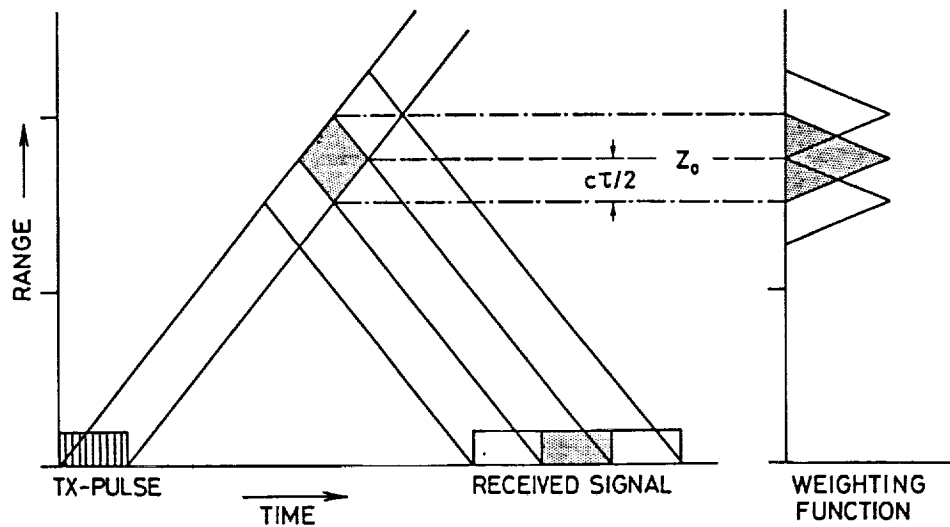

Fig. 7. Time-height chart and sampling weight when a rectangular pulse is transmitted.

The effective direction of radar echoes is usually assumed to be aligned with the antenna bore-sight direction. Therefore, the height of the radar sampling volume can be calculated by multiplying the range times $\cos\theta$ as shown in Fig. 8. In the vertical direction, the height resolution is the same as the range resolution. On the other hand, since the sampling volume for an oblique antenna beam is inclined to the horizon, the vertical distance between the highest and lowest points of the sampling volume is usually larger than the range resolution. That is, $\Delta R \cos\theta$ is not necessarily equal to ΔH as shown in Fig. 8.

Fig. 8. The sampling volume for an oblique antenna beam.

The actual shape of the sampling volume depends on the exact shape of the transmitted pulse and antenna gain pattern. Fig. 9 shows an example of the weighting function at a range of 10 km when the pulse length and half-power, full-width antenna beam width are 1 μs and 3.7°, respectively. In order to optimize the range resolution, the pulse width should be as short as possible within the limitations of the radar system. However, the height resolution in oblique directions may not be improved by shortening the transmitted pulse width when the antenna beam is not narrow enough.

So far we have assumed that radar scatterers are uniformly distributed in the radar sampling volume. In the real atmosphere, scatterers are sometimes horizontally stratified in layers with thicknesses thinner than the sampling volume. When these thin layers are distributed unevenly in the sampling volume, the effective antenna direction becomes different from the antenna bore-sight direction, which causes an error in converting from range to altitude [e.g, Fukao et al., 1988; May et al., 1988].
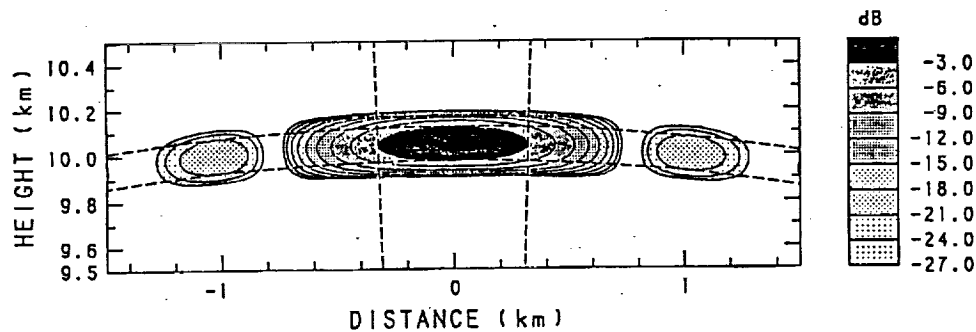

Fig. 9. The sampling weight for MU radar observations when the transmitted pulse width and half-power, full-width beam width are 1 μs and 3.7°, respectively.

In the lower stratosphere scattering from stratified layers is usually not isotropic, but has characteristics of specular reflection. In this case, the effective antenna direction is determined by the product of the antenna pattern and the angular distribution of the reflectivity. This usually biases the beam direction toward the zenith. [e.g., *Röttger*, 1981; *Tsuda et al.*, 1986].

7 COHERENT INTEGRATION

The detected quadrature signals are usually integrated for many pulses in order to increase the SNR. This digital signal processing is called a coherent integration, which requires that the phase of successively received signals be consistent with that of the local reference signal.

Before proceeding to a discussion of the effects of the coherent integration, it might be useful to review briefly the concept of a χ^2-distribution, which is commonly used in expressing noise power characteristics. We first assume that a random variable x has a Gaussian probability distribution function, expressed as

$$a(x) = \frac{1}{\sqrt{2\pi}} \exp(-\frac{x^2}{2})$$ (6)

where the mean value and standard deviation are assumed to be 0 and 1, respectively. When intensities of x are integrated M times as

$$y = x_1^2 + x_2^2 + x_3^2 + \ldots + x_M^2$$ (7)

it can be shown that y has a χ^2-distribution given by

$$b(y) = \frac{(y/2)^{M/2-1} \exp(-y/2)}{2\Gamma(M/2)}$$ (8)

where $\Gamma(M/2)$ is defined as

$$\Gamma(M/2) = (\frac{M}{2} - 1)! \qquad \text{(when } M=\text{even integer)}$$

$$= (\frac{M}{2} - 1)(\frac{M}{2} - 2)\ldots\frac{1}{2}\sqrt{\pi}$$

$$\text{(when } M=\text{odd integer and } M \geq 3)$$

$$= \sqrt{\pi} \qquad \text{(when } M=1) \tag{9}$$

The mean value μ and standard deviation σ of the χ^2-distribution are

$$\mu = M$$

$$\sigma = \sqrt{2M} \tag{10}$$

Therefore, when the square of a random variable is integrated M times, the resultant mean value is increased by M, where M is called the degrees of freedom of the χ^2-distribution. It is noteworthy that the ratio between the standard deviation and mean value is

$$\frac{\sigma}{\mu} = \sqrt{\frac{2}{M}} \tag{11}$$

which means that after M of integrations, as in (7), the distribution about the mean becomes narrower.

Now we investigate the increase of the SNR after coherent integration. If N_c coherent signals with the same SNR are integrated, the resultant signal amplitude becomes N_c times that of a single value, therefore, the signal intensity is increased by N_c^2.

On the other hand, when uncorrelated noise amplitudes are integrated over N_c samples, the resultant noise power can be expressed by (7). Because we can assume that the

noise amplitude has a Gaussian distribution, the noise power follows the χ^2-distribution with degrees of freedom equal to N_c, so that the integrated noise power is increased by N_c. As a result, coherent integration over N_c pulses improves the SNR by N_c.

Coherent integration corresponds to digital filtering with a boxcar weighting in the time domain. The signal power spectrum after coherent integration becomes the product of the original IF-signal spectrum and a weighting function expressed as

$$(\sin(\frac{2\pi f}{2/\Delta t})/\frac{2\pi f}{2/\Delta t})^2 \tag{12}$$

where $\Delta t = N_c t_{IPP}$.

In order to increase the SNR, the number of coherent integrations should be selected to span the interval over which the received signals are phase coherent with each other. There are two effects that make the integration time finite: movement of the scatterers relative to each other within the radar sampling volume, and the mean motion of scatterers relative to the radar due to background wind fields.

The relative motion of the scatterers is estimated by the correlation time, which is defined as the half-power width of the auto-correlation function of the received signal. It depends on the radar wavelength, antenna beam width and altitude [Gossard and Strauch, 1983] and becomes of the order of 0.1 to 1 sec for MST radars operating at VHF or UHF (radar wavelengths ranging from 0.1 to 10 m).

As described later, the inverse of the coherent integration time corresponds to half of the maximum frequency range of the Doppler spectra. Therefore, the integration time should be short enough to determine unambiguously the maximum radial wind velocity. This condition usually puts a practical limit on the length of the coherent integration.

8 DOPPLER VELOCITY

As shown in Fig. 4 the main procedure of digital signal processing is Fourier transformation of the time series of the received signal constructed at each range gate after increasing the SNR by coherent integration.

For a monostatic radar, signals received from stationary targets have time independent phase $\psi = -2\pi(2R/\lambda)+$constant, where λ is the radar wavelength. If R increases with time because of the radial component V_R of the motion of the scatterer, the phase decreases and the time rate of change of phase becomes

$$\frac{d\psi}{dt} = -\frac{4\pi}{\lambda}\frac{dR}{dt} = -\frac{4\pi}{\lambda}V_R = -2\pi f_D \tag{13}$$

which appears as the Doppler shift from the carrier frequency of the scattered radiowave. The Doppler frequency shift is related to the radial Doppler velocity as

$$V_R = \frac{\lambda}{2}f_D \tag{14}$$

The shift is positive for motion toward the radar.

In the earth's atmosphere the horizontal wind velocity can range up to about 100 m/s near the peak of jet streams, while the vertical wind speed is only of the order of one tenth to a few m/s. Thus when radial wind velocities are sampled at zenith angles of 10 to 30°, they can be as large as 10 to 50 m/s. The Doppler spectrum should be constructed by taking into account the wind velocity resolution and the maximum unambiguous velocity.

9 DISCRETE FOURIER TRANSFORM

The Fourier transform $F(f)$ of an infinite time series $X(t)$ is defined as

$$F(f) = \int_{-\infty}^{\infty} X(t)e^{-i2\pi ft}dt \tag{15}$$

where f is the frequency. An actual signal processing system treats only a finite time series that is discretely sampled N times at intervals of Δt. Thus the total length of the time series is $T_m = N \Delta t$.

Fig. 10 shows three sinusoidal oscillations with slightly different frequencies. The vertical lines indicate sample timings. The oscillation plotted by the dashed curve has a frequency $f_N = 1/(2\Delta t)$, which is half of the sampling frequency. When an oscillation has a frequency lower than f_N, it can be detected if the sampling is continued long enough, while oscillations with frequencies higher than f_N cannot be correctly estimated. In order to specify completely a sinusoidal oscillation, at least two sampling points are needed within one cycle of the oscillation. Therefore, f_N, called the Nyquist frequency, is the highest frequency that can be unambiguously measured in a discretely sampled time series.
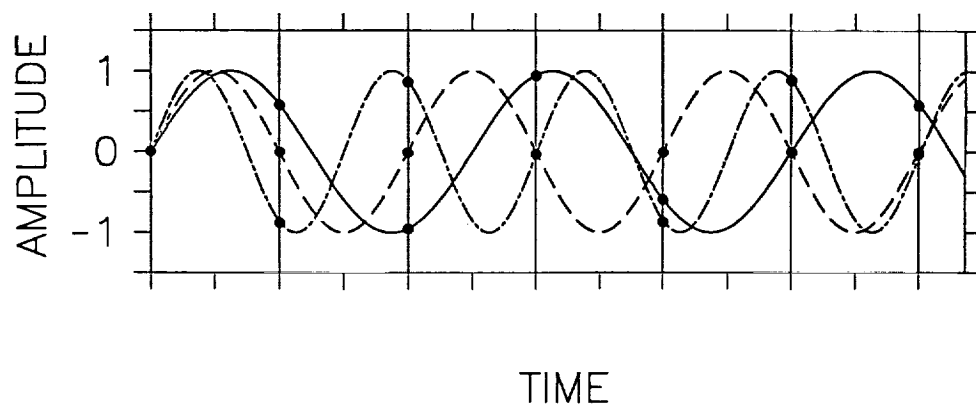

TIME

Fig. 10. Three sinusoidal signals with frequencies lower (solid), equal to (dash) and higher (dot-dash) than the sampling frequency. The sample timings are indicated by the thin vertical lines.

The Fourier transform of a discrete complex time series X_n ($n=0$ to $N-1$) is usually approximated by a finite series of harmonic functions, called a discrete Fourier transform. The coefficient of the k-th harmonic component F_k ($k=0$ to $N-1$) is defined as

$$F_k = \frac{1}{N} \sum_{n=0}^{N-1} X_n W^{nk} \tag{16}$$

while the time series of data X_n ($n=0$ to $N-1$) can be recomposed as

$$X_n = \sum_{k=0}^{N-1} F_k W^{-nk} \tag{17}$$

where

$$W = \exp(-\frac{i2\pi\Delta t}{T_m}) = \exp(-\frac{i2\pi}{N}) \tag{18}$$

Note that $F_{k+N} = F_{k-N} = F_k$, because $W^N = 1$; that is, the width of the unambiguous frequency range of a discrete Fourier transform is $2f_N$. Doppler spectra are usually plotted in a frequency range from $-f_N$ to f_N. The frequency resolution of a discrete Fourier transform then becomes $2f_N/N = 1/(N\Delta t) = 1/T_m$.

10 FREQUENCY ALIASING

We demonstrate in this section that a time series X_n sometimes cannot be related to a unique frequency because of the finite sampling resolution. We assume three oscillations with different frequencies. The dot-dash line in Fig. 11 shows an oscillation with a frequency of $0.8f_N$, while the solid and dash lines correspond to $2.8f_N$ and $-1.2f_N$, respectively, which differ by $2f_N$ in the frequency domain. When these three oscillations are sampled at the same timings indicated by the vertical lines, they produce the same data time series. This effect, which occurs when frequencies of signals are separated by an integer multiple of $2f_N$, is called a frequency aliasing.

If there are signals with frequencies outside of $\pm f_N$, they contaminate the signal within $\pm f_N$. However, because the weighting function of the coherent integration has the filter pass characteristics described by (12) and also plotted in the center panel in Fig. 12, the intensities of the components outside of $\pm f_N$ are significantly reduced, as shown in the bottom panel in Fig. 12. It should be noted that the power spectral density within $\pm f_N$ is also reduced because of the weighting. Note also that when the spectral width is large the mean Doppler shift is slightly shifted. This is due to the asymmetric weighting of the signal spectrum by the coherent integration.
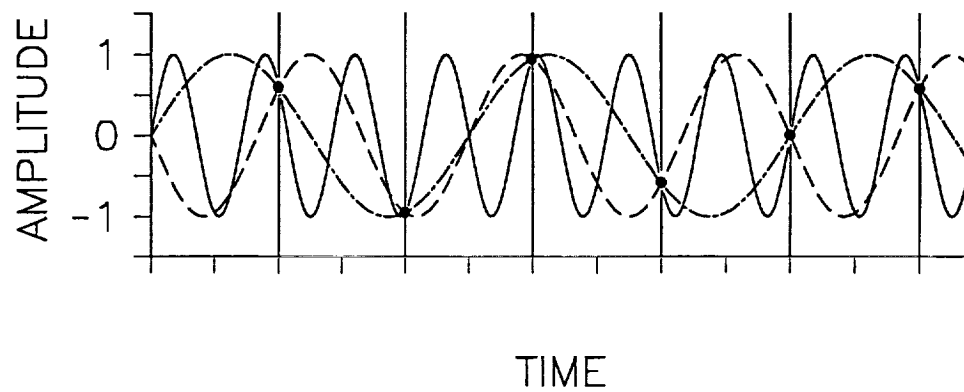

Fig. 11. The same as Fig. 10 except that the frequencies are at 0.8 (dot-dash), -1.2 (dash), and 2.8 (solid) times the Nyquist frequency (after Doviak and Zrnić, 1984).
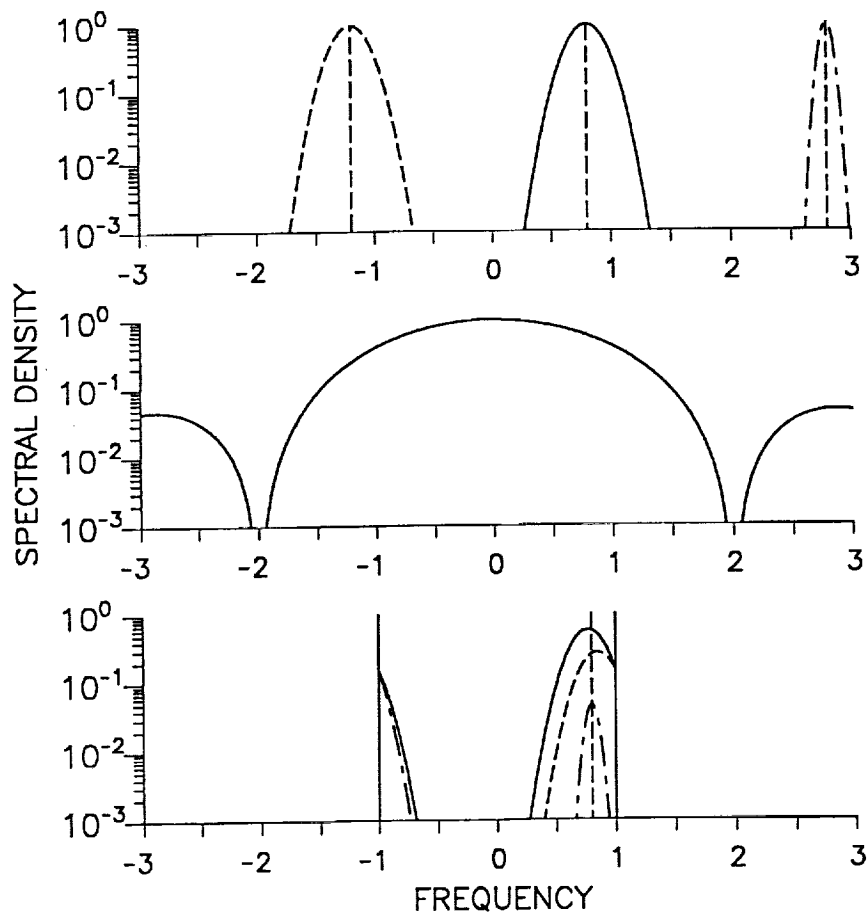
Fig. 12. Schematic diagram of frequency aliasing. The top panel shows Doppler spectra of three signals with center frequencies at $0.8f_N$ (solid), $-1.2f_N$ (dash) and $2.8f_N$ (dot-dash), where f_N is the Nyquist frequency. The center panel is the weighting function due to coherent integration, while the bottom panel shows the resultant spectrum. Vertical solid lines indicate the limits of the frequency range, while the dash line is at 0.8 f_N.

11   FAST FOURIER TRANSFORM (FFT)

Some recent MST radars have installed an array processor which is suitable for a large matrix calculations such as the discrete Fourier transform shown by Eq. (16). Most of them utilize a sophisticated technique called fast Fourier transform (FFT) [Singleton, 1967] in order to reduce computation time in analyzing the Doppler spectra.

Equation (16) indicates that N^2 multiplications are required to calculate a discrete Fourier transform. However, when N is a power of 2, part of the computation can be eliminated by using the characteristics of harmonic functions. For example, when $N = 8 = 2^3$, (16) becomes

$$NF_k = X_0 + X_1 W^k + X_2 W^{2k} + X_3 W^{3k} + X_4 W^{4k} + X_5 W^{5k} + X_6 W^{6k} + X_7 W^{7k}$$
$$= (X_0 + X_2 W^{2k} + X_4 W^{4k} + X_6 W^{6k}) + (X_1 W^k + X_3 W^{3k} + X_5 W^{5k} + X_7 W^{7k})$$

$$= (X_0 + X_2 W^{2k} + X_4 W^{4k} + \dot{X}_6 W^{6k}) + W^k (X_1 + X_3 W^{2k} + X_5 W^{4k} + X_7 W^{6k}) \quad (19)$$

which can be further rewritten as

$$F_k = \sum_{l=0}^{N/2-1} X_{2l} W^{2lk} + W^k \sum_{l=0}^{N/2-1} X_{2l+1} W^{2lk} = G_k + W^k H_k \quad (20)$$

Note that G_k and H_k are a matrix with a size of $N/2$. Therefore, total number of matrix computations becomes $2(N/2)^2$, which is reduced by a factor of 2 from (16). If $N/2$ is again a power of 2, then G_k and H_k can be further divided into smaller matrices to further reduce number of calculations. When N is a large power of 2, it can be shown that the total number of additions and multiplications to calculate an FFT increase approximately as $N \log_2 N$ and $\frac{1}{2} N \log_2 N$, respectively, which is significantly less than N^2 when N is large. The basic idea of the FFT can also be applied in cases when N is expressed by a mixed radix [Singleton, 1967].

12 INCOHERENT INTEGRATION
AND DETECTABILITY

A typical Doppler velocity spectrum is shown in Fig. 13, which was observed by the MU radar in the lower atmosphere at a zenith angle of 10°. The horizontal axis corresponds to the radial wind velocity, while the vertical axis shows relative power spectral density.

The signal is the broad enhancement centered at about 9 m/s, and the peak signal spectral density is indicated by P_S. Random fluctuations spread in frequency ranges located at the left and right of the signal are due to white noise with a mean value and standard deviation of P_N and σ_N, respectively.
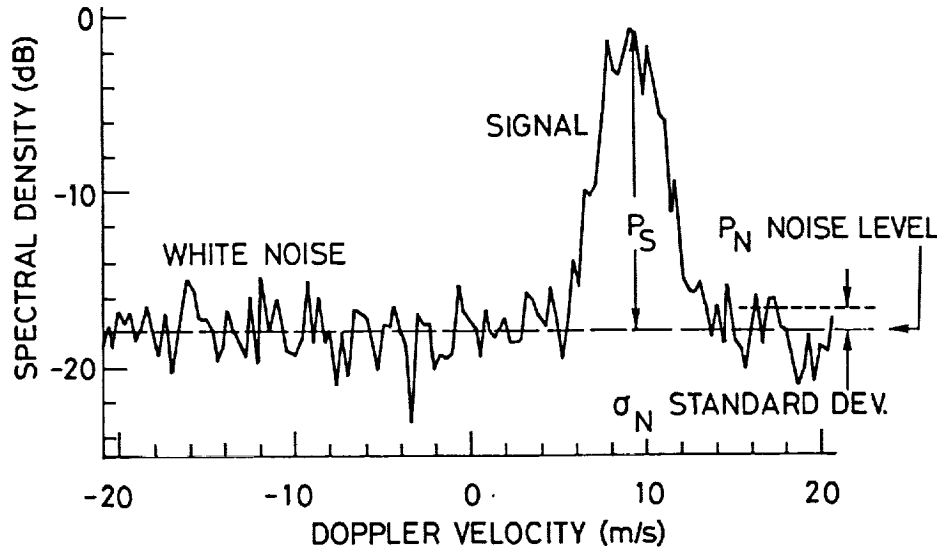
Fig. 13. A typical example of a Doppler velocity spectrum taken by the MU radar. The peak signal spectral density is indicated as P_S, while the noise level and standard deviation of noise are denoted as P_N and σ_N, respectively.

The detectability of a Doppler spectrum can be defined as

$$D = \frac{P_S}{\sigma_{S+N}} \tag{21}$$

where P_S is peak spectral density of the signal spectrum, and σ_{S+N} is standard deviation of spectral densities. When the fluctuation of the signal spectral densities is much smaller than that of the noise, (21) becomes

$$D = \frac{P_S}{\sigma_N} \tag{22}$$

which is more commonly used as a definition of the detectability [e.g., *Gage and Balsley*, 1978; *Balsley and Gage*, 1980].

The noise spectral density has a χ^2-distribution with 2 degrees of freedom, because the noise spectral density is a summation of the squares of the real and imaginary components of the amplitude spectrum, which are assumed to have a Gaussian distribution.

For a single spectrum σ_N is equal to P_N. When Doppler spectra are integrated incoherently by averaging N_i times, the mean values of the spectral densities of both the signal and noise are not changed. But, σ_N/P_N becomes $1/\sqrt{N_i}$ according to (11), because N_i incoherent integration of the noise produces a χ^2-distribution with $2N_i$ degrees of freedom. As a result, D is increased by $\sqrt{N_i}$.

Fig. 14 demonstrates the effects of incoherent integration by using a numerical simulation. The signal portion is not clearly recognizable in the spectrum plotted in the top panel in Fig. 14, which does not include any incoherent integration. On the other hand, the signal spectrum becomes easily visible in the bottom panel, which is the result of 20 incoherent integration. In normal MST radar observations, spectral parameter estimation can be done reasonably well when D is larger than about 3.
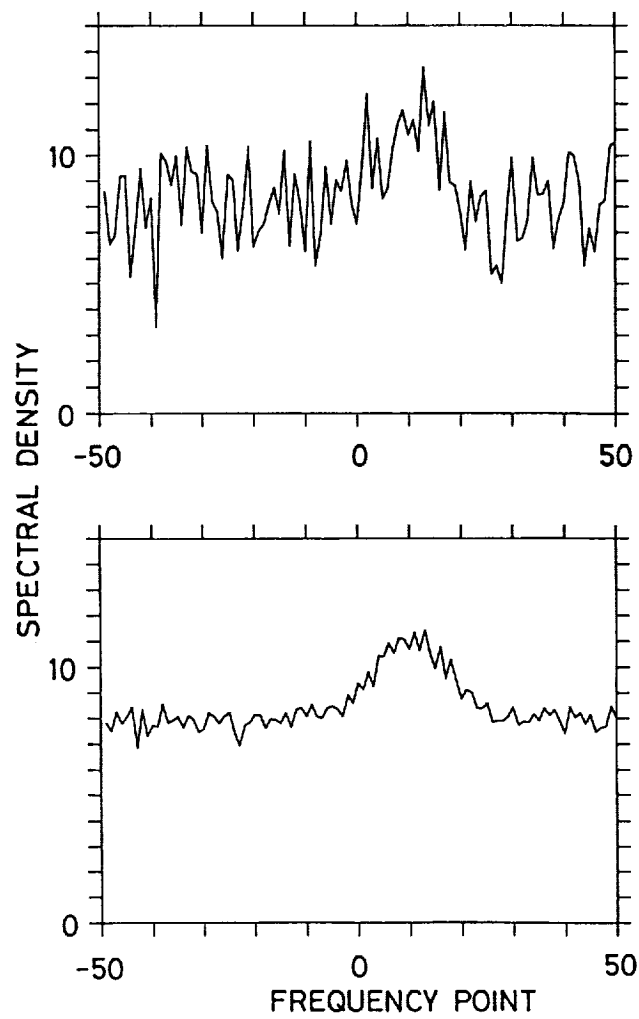
Fig. 14. Doppler spectra produced by a numerical simulation. The top panel shows a single spectrum, while the bottom panel shows a spectrum after 20 incoherent integrations.

13   NOISE LEVEL

In explaining Fig. 13 we have defined P_N as the mean value of the χ^2-distribution of the noise spectral density. A correct estimate of P_N, commonly called the noise level, is important in determining SNR, from which the characteristics of the radar scatterers such as reflectivity or reflection coefficients are derived.

Since a χ^2-distribution approaches a Gaussian distribution as its degrees of freedom becomes larger, a simple averaging of noise spectral densities might give an estimate of the noise level. However, the simple mean could be easily biased toward larger values due to spurious enhancements of the noise power by radio interference or airplane echoes.

Another estimate of the noise level can be obtained by taking the median values of the noise spectral densities. A median filter is more insensitive to spurious enhancements than simple averaging, and therefore it gives a more reliable estimate. Nevertheless, since calculation of the medians needs a large memory area and significant computation time, it cannot be practically realized in a real-time data processing systems.

We here introduce a convenient method to estimate the noise level, which can also be applied to determination of the echo power profile of incoherent scattering in the ionosphere [*Sato et al.*, 1988]. First, we need to pick up a portion of Doppler spectra that includes only noise, and separate it into K_m sub-sets each of which includes K_a spectral points. Second, in each sub-set the noise spectral densities for K_a data points are averaged. The resultant value follows a χ^2-distribution with the degree of freedom of $2K_a$. Repeat this process K_m times for all of sub-sets and get a series of averaged noise spectral densities. Finally, among these K_m determinations we need to find the minimum value P_m.

For any distribution $Q(x)$ in order for α to be a minimum, the other K_m-1 events

must have a value larger than α, whose probability β becomes

$$\beta = K_m (\int_\alpha^\infty Q(x)dx)^{K_m-1} \tag{23}$$

where the factor K_m appears because we do not specify the order of occurrence of the events.

The expectation of the minimum value can be given by calculating the first moment as follows

$$e = \int_{-\infty}^\infty \alpha Q(\alpha) K_m (\int_\alpha^\infty Q(x)dx)^{K_m-1} d\alpha \tag{24}$$

When $Q(x)$ is a normalized Gaussian distribution with a mean value and standard deviation of 0 and 1, (24) can be simplified to

$$e = \int_{-\infty}^\infty \alpha Q(\alpha) K_m \frac{1}{2}(1 - Erf(\frac{\alpha}{\sqrt{2}}))d\alpha \tag{25}$$

where Erf is the error function defined as

$$Erf(y) = \frac{2}{\sqrt{\pi}} \int_0^y \exp(-t^2)dt \tag{26}$$

Note that e is always negative, since it is the expectation of the minimum value for the normalized Gaussian distribution with zero mean.

In our case $Q(x)$ is a χ^2-distribution with $2K_a$ degrees of freedom, whose mean value and standard deviation are P_N and $P_N/\sqrt{K_a}$. However, when K_a is large enough, it can be approximated by a normalized Gaussian distribution. In this approximation, the x-axis must be normalized by the standard deviation and displaced by the mean value. In summary, e for the normalized Gaussian distribution can be related to P_m as

$$P_m = P_N - |e|\frac{P_N}{\sqrt{K_a}} \tag{27}$$

which is further modified to

$$P_N = \frac{P_m}{1 - |e|/\sqrt{K_a}} \tag{28}$$

Since the denominator of (28) is a constant for fixed K_m and K_a, P_N can be estimated by a simple computation when P_m is determined from observed Doppler spectra.

The SNR is defined as the ratio between the integrated signal and the noise power. If the signal spectrum is approximated by a Gaussian distribution with a peak value and standard deviation of P_S and σ_S, the SNR becomes

$$\mathrm{SNR} = \frac{\sqrt{2\pi}\sigma_S P_S}{P_N B_D} \tag{29}$$

where B_D is the bandwidth of the Doppler spectra.

14   OBSERVATION PARAMETERS

We need to obtain a Doppler spectrum with large SNR and detectability in order to estimate easily the spectral parameters such as the SNR, mean Doppler shift and spectral width. Likewise, we need to take into account the effects of range or frequency aliasing so as to remove ambiguities in the range and velocity measurements.

Fig. 15 schematically shows the relations among observation parameters. The IPP is proportional to the maximum unambiguous range of the observation H_m. The time interval Δt of samples after coherent integration should be determined in order for the Doppler spectra to include the maximum radial wind velocity V_m expected in the observation height range. The number of coherent integrations N_{coh}, which is the ratio $\Delta t / IPP$, is required to be as large as possible to improve the SNR; that is, IPP should be as short as possible, and Δt should be as long as possible.

The velocity resolution ΔV of a Doppler spectrum in c/s is equal to the inverse of the maximum time length T_m of the data samples. The number of FFT points N_{FFT}, which is determined by dividing T_m by ΔT, needs to be a power of 2. Since ΔV does not

necessarily correspond to the velocity resolution of a spectral parameter estimation, ΔV could be adjusted in order to get an appropriate value of N_{FFT}.
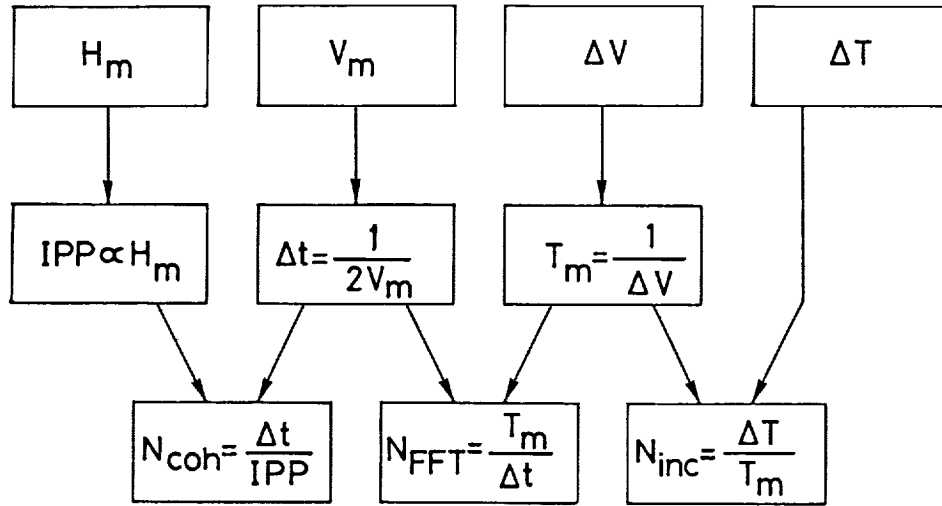

Fig. 15. The relations among observation parameters. H_m and V_m are the maximum range and radial velocity, respectively. Δt is the interval of data sampling. The minimum unit of the Doppler velocity spectrum is ΔV, while T_m is the total length of data samples. ΔT corresponds to a time resolution of Doppler spectra. N_{coh}, N_{FFT} and N_{inc} are the number of coherent integrations, FFT points and incoherent integrations, respectively.

The time resolution Δt of the spectral parameter estimation ranges from a few minutes to several hours, depending on the time scale of the phenomena to be detected by the MST radar observations. The number of incoherent integrations N_{inc} is the ratio of ΔT to T_m, which is required to be larger than about 10. Because the observation parameters are closely related to each other, we may need some experience to find a set of optimum observation parameters.

This chapter is concentrated on the description of basic concepts of the digital signal processing used in normal MST radar observations. The author hopes it will contribute to the understanding of Doppler spectra and stimulate further MST radar observations.

References

Balsley, B. B., and K. S. Gage, The MST radar technique: Potential for Middle Atmosphere Studies, *Pure and Appl. Geophys.*, *118*, 452-493, 1980.

Barton, D. K., *Radar System Analysis*, Artech House, Dedham, 1976.

Bendat, J. S., and A. G. Piersol, *Random Data: Analysis and Measurement Procedures*, John Wiley & Sons, Inc., 1971.

Cook, C. E., and M. Bernfeld, *Radar Signals, An Introduction to Theory and Applications*, Academic Press, New York, 1967.

Doviak, R. J., and D. S. Zrnić, *Doppler Radar and Weather Observations*, Academic Press, Orlando, 1984.

Fukao, S., T. Sato, P. T. May, T. Tsuda, S. Kato, M. Inaba, and I. Kimura, A systematic error in MST/ST radar wind measurement induced by a finite range volume effect, 1. Observational results, *Radio Sci.*, *23*, 59-73, 1988.

Gage, K. S., and B. B. Balsley, Doppler Radar Probing of the Clear Atmosphere, *Bull. Amer. Met. Soc.*, *59*, 1074-1093, 1978.

Gold, B., and C. M. Rader, *Digital Processing of Signals*, McGraw-Hill, Inc., 1969.

Gossard, E. E., and R. G. Strauch, *Radar Observation of Clear Air and Clouds*, Elsevier Sci. Publ., Amsterdam, 1983.

Kato, S., T. Ogawa, T. Tsuda, T. Sato, I. Kimura, and S. Fukao, The middle and upper atmosphere radar: First results using a partial system, *Radio Sci.*, *19*, 1475-1484, 1984.

May, P. T., S. Fukao, T. Tsuda, T. Sato, and S. Kato, The effect of thin scattering layers on the determination of wind by Doppler radars, *Radio Sci.*, *23*, 83-94, 1988.

Röttger, J., Investigations of lower and middle atmosphere dynamics with spaced antenna drift radars, *J. Atmos. Terr. Phys.*, *43*, 277-292, 1981.

Sato, S., A. Ito, W. L. Oliver, S. Fukao, T. Tsuda, S. Kato, and I. Kimura, Ionospheric incoherent scatter measurements with the MU radar: Techniques and capability, *Radio Sci.*, in press, 1989.

Skolnik, M. I., *Introduction to Radar Systems*, McGraw-Hill Inc., Tokyo, 1981.

Singleton, R. C., On computing the fact Fourier transform, *Commun. ACM*, *10*, 647-654, 1967.

Tsuda, T., T. Sato, K. Hirose, S. Fukao, and S. Kato, MU radar observations of the aspect sensitivity of backscattered VHF echo power in the troposphere and lower stratosphere, *Radio Sci.*, *21*, 971-980, 1986.